ANALYSIS OF THE MECHANICAL BEHAVIOR OF TIMBER-CONCRETE COMPOSITE BEAMS THROUGH FEM MODEL

Felipi Pablo Damasceno Fernandes

Emerson Felipe Félix

Jorge Munaiar Neto

Rogério Carrazedo

fpd-fernandes@usp.br

emerson.felipe.felix@gmail.com

jmunaiar@sc.usp.br

rogcarrazedo@sc.usp.br

University of São Paulo at São Carlos School of Engineering

Av. Trabalhador São-Carlense, 400, CEP 13566-590, São Carlos, São Paulo, Brasil

Abstract. *The civil constructions demands as well as technological advances provided the creation of new materials arrangements for the structural use, such as the combination of timber beams and reinforced concrete slabs through shear connectors, forming composites structures. The timber-concrete composite structures have a wide field of application, such as the construction of bridges and new buildings as well as the revitalization of old buildings. It is a competitive and flexible construction technique that, however, lacks a specific design method. Thus, this paper intends to analysis the mechanical behavior of timber-concrete composite beams using the Finite Element Method (FEM). For modelling the composites beams, it is applied the positional finite element method at the mesoscopic level, whose purpose is the nonlinear geometric analysis of bi-dimensional elastic structures made of composite materials. The results of the numerical model are compared with practical example and theoretical formulation which demonstrate the accuracy and applicability of the FEM particulate model to simulate and analysis timber-concrete composite structures.*

Keywords: *Timber-Concrete beam, Composite, Finite Element Method, Positional FEM*

1 INTRODUCTION

The timber-concrete composite beam consists of a structural arrangement formed by the union of a timber joist to a reinforced concrete slab through shear connector, taking advantage of the best properties of the materials in bending: timber resists to tensile stresses while concrete resists to compression efforts. The timber-concrete composite beam has a wide application field, which can be highlighted its use in bridges superstructures, revitalization of old buildings, as well as the construction of new buildings.

When compared to others structural systems, timber-concrete composite structures have several advantages. Regarding timber floors, the timber-concrete composite beam is more rigid and has better acoustic and thermal insulation. Compared to conventional reinforced concrete structures, they are lighter, faster-erected and more economical (Yeoh et al., 2011).

The bond mechanical behavior has a direct influence on the most important mechanical properties of the composite system, namely load-carrying capacity, stiffness and ultimate deformation capacity. Among the bond properties, the ones with the greatest influence on the mechanical behavior of the composite system are the load-carrying capacity, stiffness and ductility (Sebastian, 2003; Dias et al., 2007; Dias et al., 2010).

The standard which is used to design timber-concrete composite structures is Eurocode 5 (2004). This standard stablishes the Mohler model, also known as equivalent beam model, for the design of "T" beams composed of two elements, since the stresses in the constituent materials remain within the elastic regime. On the other hand, the ductility of the bond is not considered in this calculation method, neither directly nor indirectly. Regardless of this factor, this property might has a significant influence on the system's mechanical behavior (Dias and Jorge, 2011).

However, the presented Eurocode 5 (2004) approach is limited by the following assumptions: the members have constant sections, the applied load has a sinusoidal distribution in order to have exact solutions, and the materials and joints are linear elastic. Other models have been developed to overcome these limitations.

Another way to analyze timber-concrete composite beams is using numerical approaches, as the Finite Element Method (FEM). Molina (2008) and Molina and Calil Junior (2009 represented the behavior of timber-concrete composite elements using the commercial Finite Element Program ANSYS. They observed that representing timber as an isotropic material leads to inaccurate results, while using an orthotropic constitutive behavior provides results with a relative error of 15% when compared to experimental investigations. Also using FEM models to simulate timber-concrete composite structures, Dias (2005) and Dias et al. (2007) noticed that the global behavior of these elements was overestimated by numerical models, showing higher initial stiffness.

With the purpose to model the mechanical behavior of timber-concrete composite structures in a better way, a particulate FEM approach was used in this work. The formulation is developed in mesoscopic level, aiming a geometric non-linear analysis of two-dimensional elastic structures composed of particulate composite materials. The results of the numerical model are compared with practical example that demonstrate the accuracy and its applicability to simulate timber-concrete composite structures.

2 MATERIALS AND METHODS

Initially, the direct FEM particulate approach for modeling reinforced elastic solids is presented, the formulation was proposed by Paccola and Coda (2016). The model is responsible to represent the mechanical behavior of composite/particulate materials, as timber-concrete composite. Then it is described the Theoretical model to determine the mechanical behavior of timber-concrete structures. The theoretical model is described in Eurocode 5 (2004) and is based on the influence of slip between timber and concrete through an effective bending stiffness.

2.1 FEM particulate approach

To represent the mechanical behavior of any phase of the particulate composite, a direct FEM based on positions (PFEM), proposed by Paccola and Coda (2016) was used. We started the description from the total energy stationary principle and describe the formulation of the PFEM. In the absence of dissipative potentials and considering static applications, the total energy of any solid and its variation are presented in the Eq. (1) and (2), respectively.

$$\prod = U + P \tag{1}$$

$$\delta\prod = \delta U + \delta P = 0 \tag{2}$$

where U is the strain energy stored in all phases of the composite and P is the potential energy of external forces (Fig. 1.a).

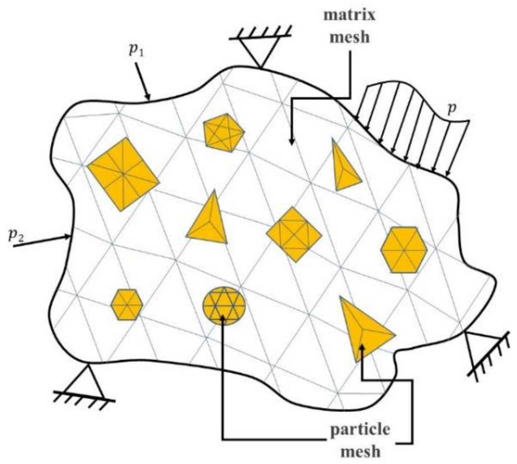

Figure 1.a. Generic body illustration and its discretization

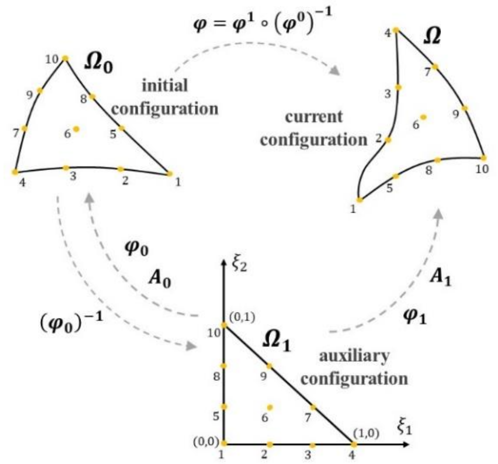

Figure 1.b. Initial and current configuration of a membrane

Considering that both matrix and particle are represented and modeled here by two-dimensional (*2D*) finite element, the initial and final body configuration from the kinematic description of a generic *2D* solid finite element as show in Fig. 1.b. The finite element configuration showed (Fig. 1.b) is merely illustrative and the formulation can be applied for any other element.

To best define the FEM formulation based in positions Paccola and Coda (2016) propose the following guide. First, the change of configuration function of a finite element by writing the associated Green strain is defined. Then, the strain energy is described. Next, the methodology to include finite element particles without the addition of new degrees of freedom in the problem is related. To finalize, they include the potential of the external conservative forces and apply the total energy stationary principle resulting in the nonlinear equilibrium equations. To solve the nonlinear equations, the Newton-Raphson procedure is used achieving the searched solution.

2.1.1 Change of configuration function

The Fig. 1.b represents the initial configuration of a finite element of any phase of the composite Ω_0 and represents its current configuration Ω. The auxiliary configuration Ω_1 is used to generate the Lagrange polynomials ϕ_j that compose the initial and currents mappings, as showed in the Eq. (3) and (4).

$$x_i = \varphi_i^0 = \phi_j(\xi_1, \xi_2) X_i^j \tag{3}$$

$$y_i = \varphi_i^1 = \phi_j(\xi_1, \xi_2) Y_i^j \tag{4}$$

where X_i^j and Y_i^j refer to the initial and current nodal positions, respectively. The term *i* refers to the finite element nodes and *j* their directions and degree of freedom.

Then, in the Eq. (5) the current configuration is determined using the initial and auxiliary mappings. The gradient of the change of configuration function, that will be used here to determinate the deformation function, is showed in Eq. (6). In the Eq. (7) the gradients of the mappings, i.e., $\boldsymbol{A^1}$ and $\boldsymbol{A^0}$ are determined.

$$\varphi = \varphi^1 \circ (\varphi^0)^{-1} \tag{5}$$

$$Grad(\vec{\varphi}) = Grad(\vec{\varphi}^1) \cdot (Grad(\vec{\varphi}^0))^{-1} = \boldsymbol{A}^1 \cdot (\boldsymbol{A}^0)^{-1} \tag{6}$$

$$\boldsymbol{A}^0 = \frac{\partial \varphi^0}{\partial \xi} = \phi \cdot \vec{X} \quad and \quad \boldsymbol{A}^1 = \frac{\partial \varphi^1}{\partial \xi} = \phi \cdot \vec{Y} \tag{7}$$

where $Grad(\cdot)$ represent the gradient of a function, $\boldsymbol{A^1}$ and $\boldsymbol{A^0}$ are the gradients mappings ξ and refers to the dimensionless coordinates of the auxiliary configuration.

2.1.2 Energy strain

From the gradients of the mappings, Eq. (7), and the deformation gradient, Eq. (6), the Green strain cab be determinate, as showed in Eq. (8).

$$\boldsymbol{E} = \frac{1}{2}(\boldsymbol{A}^t \cdot \boldsymbol{A} - \boldsymbol{I}) = \frac{1}{2}(\boldsymbol{C} - \boldsymbol{I}) \tag{8}$$

where $\boldsymbol{E}$ is the Green strain, $\boldsymbol{I}$ is the identity matrix and $\boldsymbol{C}$ is the Cauchy-Green stretch tensor.

From the Green strain one writes the expressions of the specific strain energy, which defines, respectively, the plane stress, Eq. (9), or the plane strain Saint-Venant-Kirchhoff constitutive laws, Eq. (10).

$$u^{pStress} = \frac{1}{2}[K(\boldsymbol{E}_{11}^2 + \boldsymbol{E}_{22}^2) + 2\upsilon K(\boldsymbol{E}_{11}E_{22}) + 2G(\boldsymbol{E}_{12}^2 + \boldsymbol{E}_{21}^2)] \tag{9}$$

$$u^{pStrain} = \frac{1}{2}[(1-\upsilon)\overline{K}(\boldsymbol{E}_{11}^2 + \boldsymbol{E}_{22}^2) + 2\upsilon\overline{K}(\boldsymbol{E}_{11}\boldsymbol{E}_{22}) + 2G(\boldsymbol{E}_{12}^2 + \boldsymbol{E}_{21}^2)] \tag{10}$$

where $K = \frac{\mathfrak{E}}{(1-\upsilon^2)}$, $\overline{K} = \frac{\mathfrak{E}}{(1+\upsilon)(1-2\upsilon)}$, $G = \frac{\mathfrak{E}}{2(1+\upsilon)}$, $\mathfrak{E}$ is the longitudinal elastic modulus and υ is the Poisson ratio.

It can be observed in the Eq. (7) to (10) that, in a finite element the specific strain energy is a function of the current positions of nodes, the same goes for any solid considering matrix and particles (Paccola and Coda, 2016).

Thus, the strain energy for any solid is obtained integrating the Eq. (9) or (10) in your volume Eq. (11). Then, the strain energy of a whole body is the sum of all energies developed over finite elements.

$$U = \int_{V_0} u(\vec{Y})dV_0 \tag{11}$$

With the strain energy, Eq. (11), two another quantity of interest for the simulation process can be obtained, the internal force, Eq. (12), and the Hessian matrix, Eq. (13). Both equations are determinated with the variational calculus and using the chain rule, from a trial position, $\vec{Y}$.

$$\overrightarrow{F_{int}} = \frac{\partial U}{\partial \vec{Y}} = \int_{V_0} \frac{\partial u}{\partial \boldsymbol{E}} : \frac{\partial \boldsymbol{E}}{\partial \vec{Y}} dV_0 = \int_{V_0} \boldsymbol{S} : \frac{\partial \boldsymbol{E}}{\partial \vec{Y}} dV_0 \tag{12}$$

$$\boldsymbol{H} = \frac{\partial^2 U}{\partial \vec{Y} \partial \vec{Y}} = \frac{\partial}{\partial \vec{Y}} \int_{V_0} \frac{\partial u}{\partial \boldsymbol{E}} : \frac{\partial \boldsymbol{E}}{\partial \vec{Y}} dV_0 = \int_{V_0} \left(\frac{\partial \boldsymbol{E}}{\partial \vec{Y}} : \frac{\partial^2 u}{\partial \boldsymbol{E} \partial \boldsymbol{E}} : \frac{\partial \boldsymbol{E}}{\partial \vec{Y}} + \boldsymbol{S} : \frac{\partial^2 \boldsymbol{E}}{\partial \vec{Y} \partial \vec{Y}} \right) dV_0 \tag{13}$$

where $\overrightarrow{F_{int}}$ is the internal force, $\boldsymbol{S}$ refers to the second Piola-Kirchhoff stress and $\boldsymbol{H}$ is the Hessian matrix.

2.1.3 Particles inclusion via kinematics compatibility

This section, presents the strategy used by Paccola and Coda (2016) to include finite particles in the matrix without adding degrees of freedom.

The principal premises of the formulation is that the position of particle node is written as a function of the position of the nodes of a solid finite element, which the particle belongs. To accomplish this operation, the perfect adhesion between particle and solid and divided the strain energy stored in solid and particle is considered.

As previously mentioned it is necessary to write the particle nodal positions as a function of the solid finite element nodes positions. In order to do so we will use the shape functions of the solid finite element. Thus, it is necessary to know the dimensionless coordinates $\left(\xi_1^p, \xi_2^p\right)$ of the particles nodes at the initial configuration of the problem. This is done by solving the system of nonlinear equations, Eq. (14), with Newton-Raphson procedure, which can be seen in Paccola and Coda (2016).

$$X_{Pi} = \phi_l\left(\xi_1^p, \xi_2^p\right) X_{li} \tag{14}$$

in which ϕ_l are the solid finite element shape functions, X_{Pi} are the initial coordinates of particle node *P* generated regardless of the solid mesh and X_{li} are the finite element nodes that contains the particle node.

Knowing the solid finite element shape functions and the current nodal positions of the matrix, the value of all particles nodal positions is determined as showed in Eq. (15).

$$Y_{Pi} = \phi_l\left(\xi_1^p, \xi_2^p\right) Y_{li} \tag{15}$$

where Y_{Pi} are the current coordinates of particle node *P* generated regardless of the solid mesh and Y_{li} are the current positions of the solid nodes.

In order to complete the necessary kinematical relations to be used in the proposed connection it is necessary to derive the particles coordinates regarding solid coordinates, as showed in the Eq. (16). The Eq. (16) shows that, when the particle node belongs to the solid finite element, the term $\partial Y_{pi} / \partial Y_{\beta\alpha} = \phi_\beta\left(\xi_1^p, \xi_2^p\right)$ if the direction α of the solid position is equal to direction *i* of the analyzed particle.

$$\frac{\partial Y_{pi}}{\partial Y_{\beta\alpha}} = \frac{\partial Y_{li}}{\partial Y_{\beta\alpha}} \phi_l\left(\xi_1^p, \xi_2^p\right) = \delta_{\alpha i}\delta_{\beta l}\phi_l\left(\xi_1^p, \xi_2^p\right) = \delta_{\alpha i}\phi_\beta\left(\xi_1^p, \xi_2^p\right) \tag{16}$$

in which the particle node belongs to the solid finite element, Y_{Pi} are the current coordinates of particle node *P* generated regardless of the solid mesh and Y_{li} are the current positions of the solid nodes.

To establish the contribution of the particles in the composite it was divide the strain energy, written in Eq. (1), in two parts, one due to the matrix and one due to the particles. It is important to mention that each particle can have any shape and be made of different material. Thus, the total energy is written in the Eq. (17), which provides with some mathematical manipulation the internal force and Hessian matrix for a composite solid (matrix + particles). Both Eq. (18) and (19) were obtained by deriving the Eq. (17) in function of the nodes positions.

$$U = U_{mat} + U_{part} \tag{17}$$

$$\vec{F_i} = \frac{\partial\left(U_{mat} + U_{part}\right)}{\partial Y_{\beta\alpha}} = \frac{\partial U_{mat}}{\partial Y_{\beta\alpha}} + \frac{\partial U_{part}}{\partial Y_{pi}} \frac{\partial Y_{pi}}{\partial Y_{\beta\alpha}} \tag{18}$$

$$H_{\beta\alpha\eta\gamma} = \frac{\partial^2\left(U_{mat} + U_{part}\right)}{\partial Y_{\beta\alpha}\partial Y_{\eta\gamma}} = \int_{V_0} \frac{\partial^2 u_{mat}}{\partial Y_{\beta\alpha}\partial Y_{\eta\gamma}} dV_0 + \int_{{V_0}^p} \frac{\partial^2 u_{part}}{\partial Y_{\beta\alpha}\partial Y_{\eta\gamma}} d{V_0}^{part} \tag{19}$$

As the last term in the Eq. (19) corresponds to the particles, the chain rule are applied making an automatic correspondence of the particles degrees of freedom and the matrix degrees of freedom, as showed in the Eq. (20).

$$\begin{aligned}\frac{\partial^2 u_{part}}{\partial Y_{\beta\alpha}\partial Y_{\eta\gamma}} &= \frac{\partial^2 u_{part}}{\partial Y^p_{\rho\omega}\partial Y^p_{\rho w}}\frac{\partial Y^p_{\rho\omega}}{\partial Y_{\beta\alpha}}\frac{\partial Y^p_{\rho w}}{\partial Y_{\eta\gamma}} + \frac{\partial^2 u_{part}}{\partial Y^p_{\rho\omega}\partial Y^p_{\theta\pi}}\frac{\partial Y^p_{\rho\omega}}{\partial Y_{\beta\alpha}}\frac{\partial Y^p_{\theta\pi}}{\partial Y_{\eta\gamma}} \\ &+ \frac{\partial^2 u_{part}}{\partial Y^p_{\theta\pi}\partial Y^p_{\rho\omega}}\frac{\partial Y^p_{\theta\pi}}{\partial Y_{\beta\alpha}}\frac{\partial Y^p_{\rho\omega}}{\partial Y_{\eta\gamma}} + \frac{\partial^2 u_{part}}{\partial Y^p_{\theta\pi}\partial Y^p_{\theta\pi}}\frac{\partial Y^p_{\theta\pi}}{\partial Y_{\beta\alpha}}\frac{\partial Y^p_{\theta\pi}}{\partial Y_{\eta\gamma}}\end{aligned} \tag{20}$$

where the index P indicate the particle nodes.

2.1.4 Solution Process

Considering conservative nodal external forces and the strain energy divided in parts corresponding to the matrix and particles, Eq. (17), the total potential energy is now write in the Eq. (21), and applying the stationary principle results in the Eq. (22).

$$\prod = U_{mat} + U_{part} + P = U_{mat} + U_{part} - \vec{\mathrm{F}}_{ext} \cdot \vec{\mathrm{Y}} \tag{21}$$

$$\delta\prod = \left[U_{mat} + U_{part} - \vec{\mathrm{F}}_{ext} \cdot \vec{\mathrm{Y}}\right] \cdot \delta\vec{\mathrm{Y}} = \vec{0} \tag{22}$$

where $\vec{\mathrm{F}}_{ext}$ is the external forces applied in the solid.

Applying Eq. (12) and Eq. (18) and considering arbitrary the variation, the nonlinear equilibrium equation results in the Eq. (23). As the Eq. (23) is nonlinear, from a trial position, near to the solution, one can make a Taylor expansion to the first order, as showed in Eq. (24).

$$\mathrm{g}(\vec{\mathrm{Y}}) = \vec{\mathrm{F}}_{int}(\vec{\mathrm{Y}}) - \vec{\mathrm{F}}_{ext} = \vec{0} \tag{23}$$

$$g(\vec{\mathrm{Y}}) = g(\vec{\mathrm{Y}}^{trial}) + \left.\frac{\partial g(\vec{\mathrm{Y}})}{\partial\vec{\mathrm{Y}}}\right|_{\vec{\mathrm{Y}}^{trial}} \cdot \Delta\vec{\mathrm{Y}} = 0 \tag{24}$$

$$\Delta\vec{\mathrm{Y}} = -\left(\left.\frac{\partial g(\vec{\mathrm{Y}})}{\partial\vec{\mathrm{Y}}}\right|_{\vec{\mathrm{Y}}^{trial}}\right)^{-1} \cdot g(\vec{\mathrm{Y}}^{trial}) = -\mathbf{H}^{-1} \cdot g(\vec{\mathrm{Y}}^{trial}) \tag{25}$$

Solving the linear Eq. (24) one finds the position correction $\Delta\vec{\mathrm{Y}}$, Eq. (25), and the trial position is corrected by $\vec{\mathrm{Y}}^{trial} = \vec{\mathrm{Y}}^{trial} + \Delta\vec{\mathrm{Y}}$ until convergence when assumes that $\vec{\mathrm{Y}} = \vec{\mathrm{Y}}^{trial}$ is the solution of the problem.

2.2 Theoretical Model

The design of timber-concrete composite beams, according to Eurocode 5 (2004), is based on the influence of slip between timber and concrete through an effective bending stiffness, shown in Eq. (26).

$$(EI)_{ef} = E_c.I_c + \gamma_c.E_c.A_c.a_c^2 + E_w.I_w + \gamma_w.E_w.A_w.a_w^2 \tag{26}$$

Proceedings of the XXXVIII Iberian Latin-American Congress on Computational Methods in Engineering
P.O. Faria, R.H. Lopez, L.F.F. Miguel, W.J.S. Gomes, M. Noronha (Editores), ABMEC, Florianópolis, SC, Brazil, November 5-8, 2017.

In the Eq. (26), $(EI)_{ef}$ is the effective bending stiffness, E_c is the modulus of elasticity of concrete in compression, I_c is the second moment of area of concrete section, γ_c is the factor of reduction of the inertia of concrete, Eq. (27), A_c is the area of concrete section, a_c is the distance of the centroid of concrete area to neutral line, Eq. (28), E_w is the modulus of elasticity of timber in compression, I_w is the second moment of area of timber section, γ_w is the factor of reduction of the inertia of timber, equal to 1.0, A_w is the area of timber section, a_w is the distance of the centroid of timber area to neutral line, Eq. (29).

$$\gamma_c. = \left[1 + \frac{\pi^2.E_c.A_c.s}{K.L^2}\right] \tag{27}$$

In Eq. (27), s is the spacing between connectors, K is the slip modulus under service, Eq. (30) and L is the span of the beam.

$$a_c = \left[\frac{h_c + h_w}{2}\right] - a_w \tag{28}$$

$$a_w = \frac{\gamma_c.E_c.A_c.(h_c + h_w)}{2.(\gamma_c.E_c.A_c + \gamma_w.E_w.A_w)} \tag{29}$$

The parameters of Eq. (28) and (29) are defined in the Fig. 2.

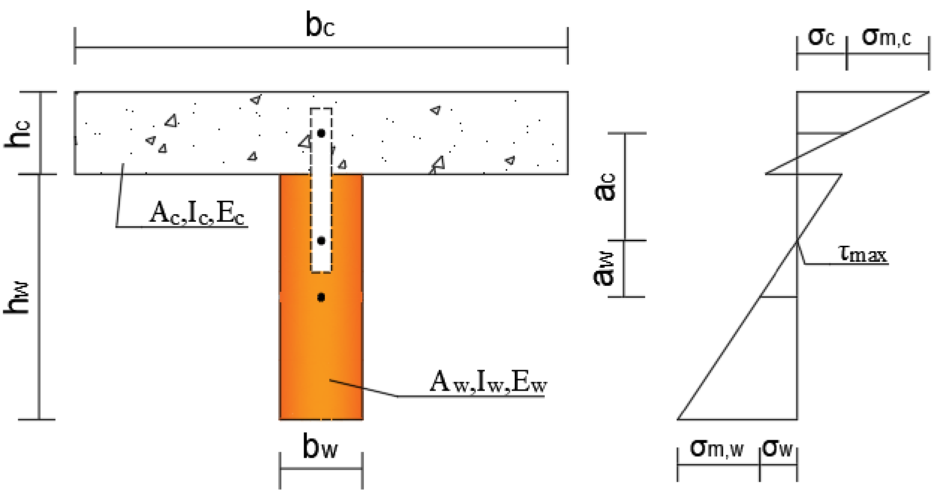

Figure 2. Timber-concrete composite beam and its stresses

For slip modulus under service defined in Eq. (30), ρ_m is the mean density of composite material (given in Eq. (31), where ρ_c is the concrete density and ρ_w is the timber density in kg/m³) and *d* is the screw diameter (mm).

Proceedings of the XXXVIII Iberian Latin-American Congress on Computational Methods in Engineering
P.O. Faria, R.H. Lopez, L.F.F. Miguel, W.J.S. Gomes, M. Noronha (Editores), ABMEC, Florianópolis, SC, Brazil, November 5-8, 2017.

$$K = \frac{\rho_m^{1.5}.d}{23} \tag{30}$$

$$\rho_m = \sqrt{\rho_c.\rho_w} \tag{31}$$

Considering M the bending moment in the section, f_c the compressive strength of concrete, σ_c the normal stress in the centroid of the concrete slab due normal force and $\sigma_{m,c}$ is the normal stress on the board of the concrete slab due bending moment, the verification of the normal compression stress on the concrete slab is made by the Eq. (32) to (34).

$$\sigma_c = \gamma_c.E_c.a_c.\frac{M}{(EI)_{ef}} \tag{32}$$

$$\sigma_{m,c} = 0.5.E_c.h_c.\frac{M}{(EI)_{ef}} \tag{33}$$

$$\sigma_c + \sigma_{m,c} \leq f_c \tag{34}$$

The verification of the bottom end of the timber beam should be made by Eq. (35) to (37).

$$\sigma_w = \gamma_w.E_w.a_w.\frac{M}{(EI)_{ef}} \tag{35}$$

$$\sigma_{m,w} = 0.5.E_w.h_w.\frac{M}{(EI)_{ef}} \tag{36}$$

$$\sigma_w + \sigma_{m,w} \leq f_w \tag{37}$$

In the above equations, σ_w is the normal stress in the centroid of the timber beam due normal force and $\sigma_{m,w}$ is the normal stress on the board of the timber beam due bending moment and f_w is the tensile strength of timber.

3 RESULTS AND DISCUSSIONS

3.1 Problem analyzed

With the purpose to verify the FEM particulate model, two composite timber-concrete beams presented by Matthiesen et al. (2010) are modeled and the results are compared with the theoretical formulation (presented in section 2.2) and the experimental results obtained by Matthiesen et al. (2010).

Both beams have 2.0 m span and are composed by a timber joist of 0.05 x 0.145 m² cross-section and a concrete slab of 0.30 x 0.05 m² cross section. The bond between concrete and timber is made by metallic pins with 12.5 mm diameter. For the beam one was used 14 connectors spaced by 0.15 m while for the beam two was used 20 connectors spaced by 0.20 m. A point load was applied on the thirds of the span (see Fig. 3). Due to its symmetry, the Fig. 4.a shows a half of the beam 1 while the Fig. 4.b shows a half of the beam 2. In Table 1 is summarized the mechanical and physical properties of the concrete slab and timber joist and metallic pins (connectors).

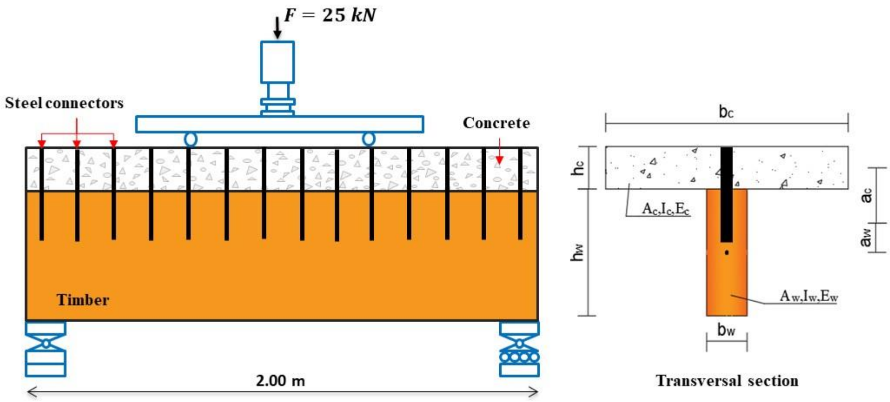

Figure 3. Timber-concrete composite beam

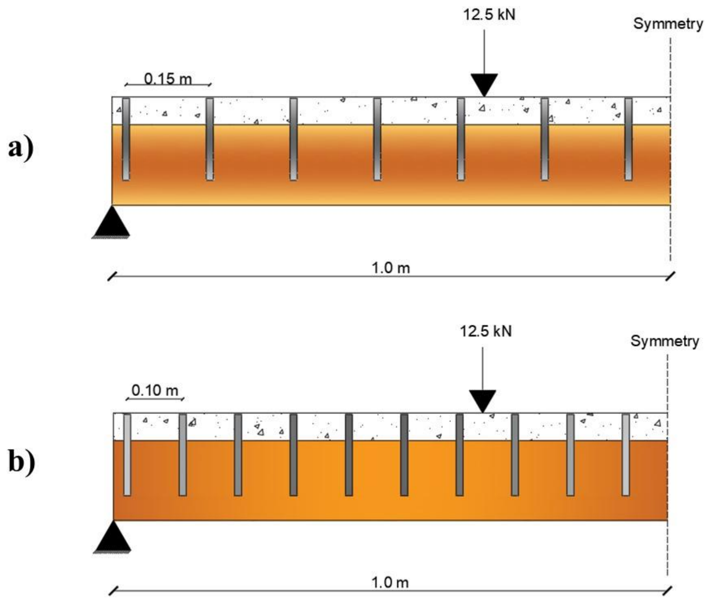

Figure 4. Geometry and design of: a) beam 1 and b) beam 2

To represent the beam, the matrix was discretized into 2470 triangular finite elements with cubic approximation, totalizing 11344 nodes and 22688 degrees of freedom (Fig. 5.a). For the representation of each connector, we adopted 78 triangular finite elements (particles) with cubic approximation, totalizing 415 nodes (Fig. 5.b). The nonlinear analysis was performed in 12 loading steps.

Table 1. Coefficients in constitutive relations

Beam	Properties				
	ρ_c (kg/m³)	ρ_w (kg/m³)	E_c (kN/m²)	E_w (kN/m²)	E_{steel} (kN/m²)
1	2500.0	838.0	3793.5	1862.6	21000.0
2	2500.0	838.0	4200.5	1770.5	21000.0

a)

b)

c)

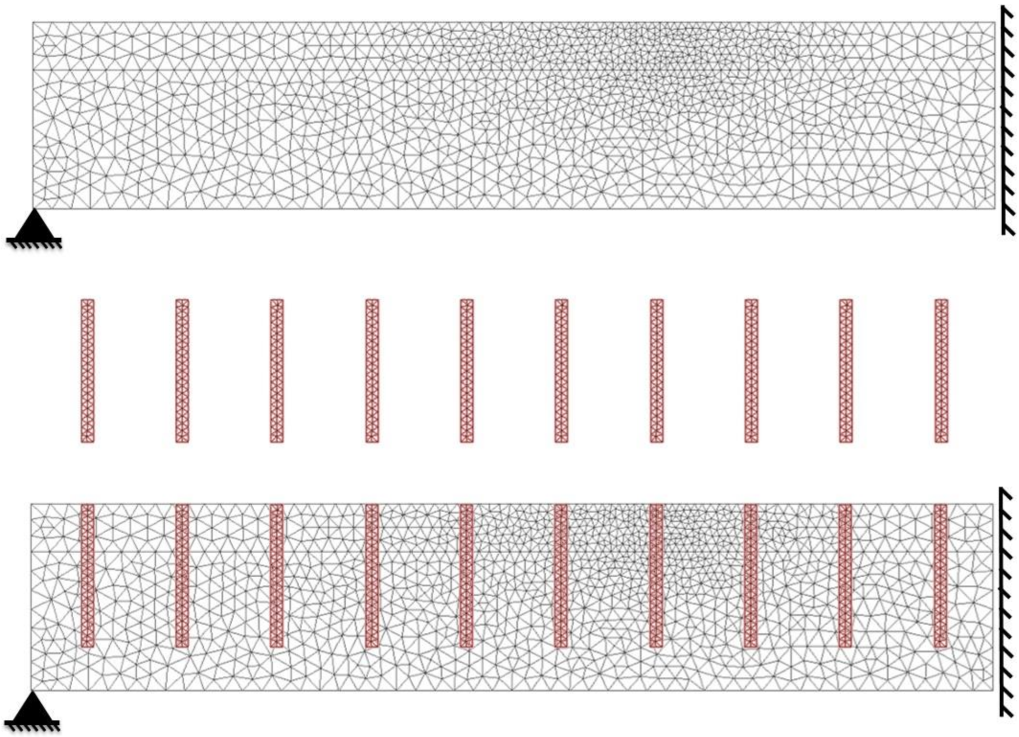

Figure 5. Mesh of: a) timber-concrete matrix; b) connectors and c) composite beam

To represent the beam, the matrix was discretized into 2470 triangular finite elements, with order of cubic approximation, totaling 11344 nodes and 22688 degrees of freedom (Fig. 5.a). For the representation of each connector, we adopted 78 triangular finite elements (particles), with order of cubic approximation, totaling 415 nodes (Fig. 5.b). The nonlinear analysis was performed in 12 loading steps.

Proceedings of the XXXVIII Iberian Latin-American Congress on Computational Methods in Engineering
P.O. Faria, R.H. Lopez, L.F.F. Miguel, W.J.S. Gomes, M. Noronha (Editores), ABMEC, Florianópolis, SC, Brazil, November 5-8, 2017.

3.2 Displacement field analysis

Figures 6 and 7 show the force versus vertical displacement curves for the beams 1 and 2, respectively. In these graphics are represented the experimental data obtained by Matthiesen et al. (2010) and the results acquired in this paper by the theoretical model and the finite element method. It can be noticed that for a force of 23 kN the beam 1 showed a vertical displacement of approximately 10 mm, while the theoretical model predicted 4 mm of vertical displacement and the finite element method indicated 11 mm. For this same force, the vertical displacement for the beam 2 was 8 mm, and the values stated by the theoretical model and the finite element method was, respectively, 5 and 9 mm.

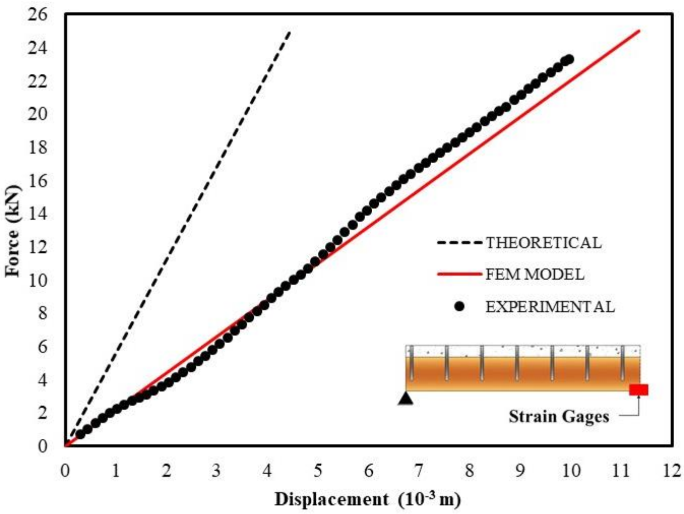

Figure 6. Vertical displacement of the beam 1

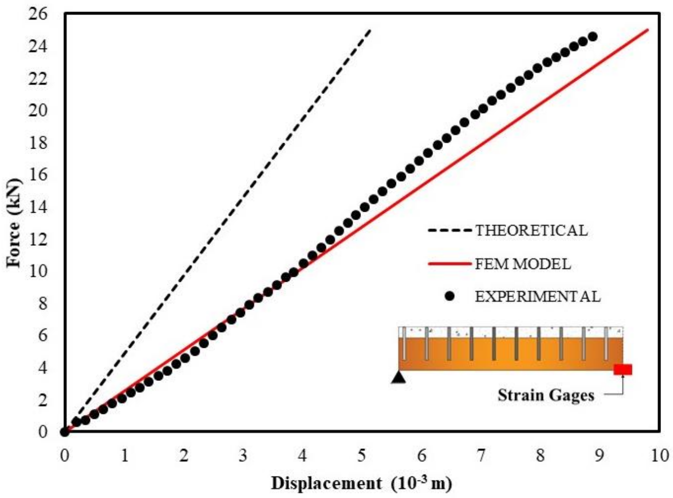

Figure 7. Vertical displacement of the beam 2

Analyzing the equations proposed by the theoretical model, it can be noted that the reduction in the spacing between the shear connectors leads to a more rigid structure and thus a lower vertical displacement. However, comparing the beams 1 and 2, it was observed that the vertical displacement for an equal force level is similar, although the spacing of the shear connector in beam 1 is 0.15 m and for beam 2 is 0.10. This fact can be explained by the huge difference between the elastic modulus of the timber joists in beam 1 and 2. Although the spacing between the metallic pins in beam 2 is lower than in the beam 1, the modulus of elasticity of the timber in this beam is just 58% of the modulus of elasticity of the timber in beam 2, leading to a less rigid structure.

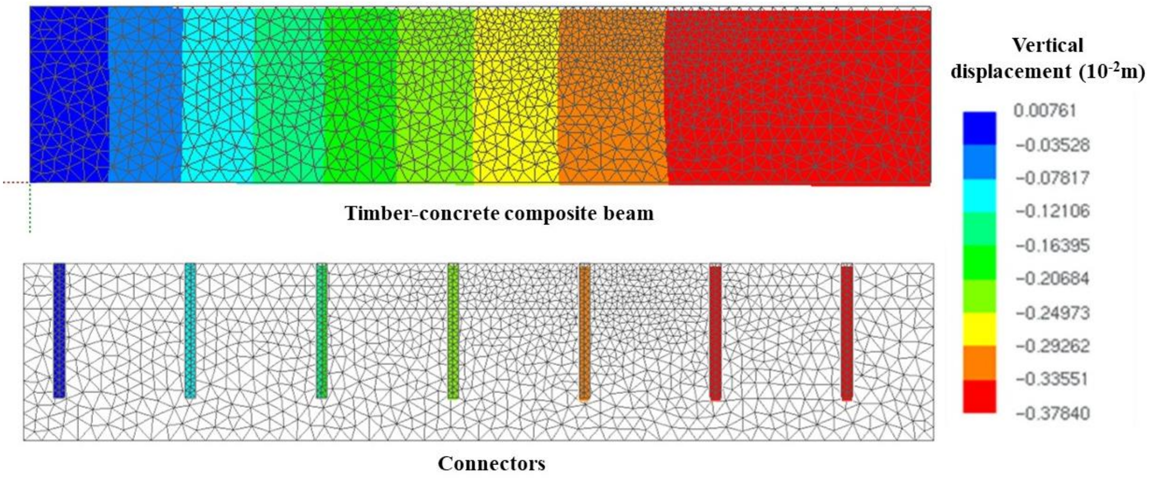

Figure 8. Vertical displacement of the beam 1 and it connectors

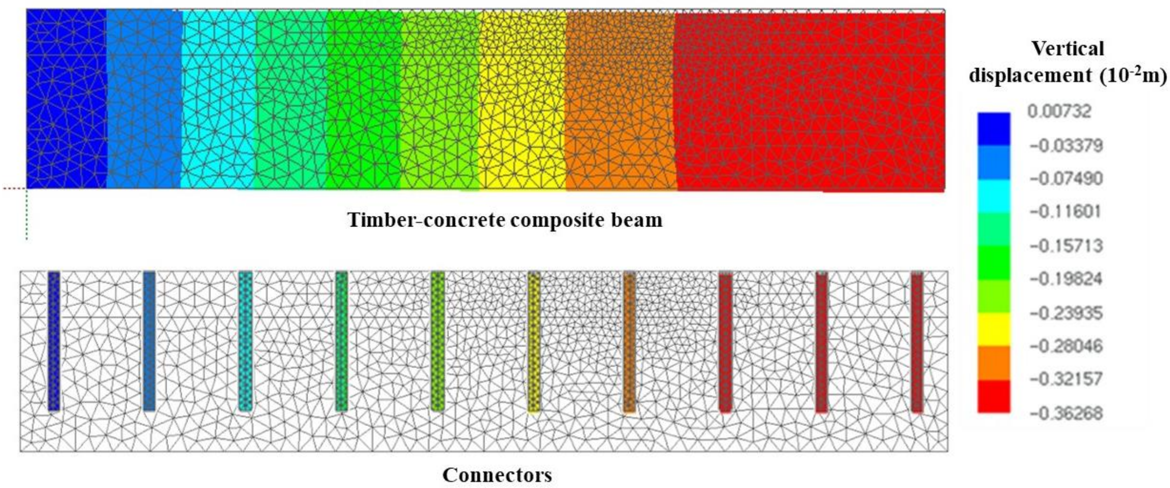

Figure 9. Vertical displacement of the beam 2 and it connectors

It can also be noted by Figs. 6 and 7 that the results presented by the theoretical model are stiffer than the experimental data, as well as the finite element formulation showed a good

Proceedings of the XXXVIII Iberian Latin-American Congress on Computational Methods in Engineering
P.O. Faria, R.H. Lopez, L.F.F. Miguel, W.J.S. Gomes, M. Noronha (Editores), ABMEC, Florianópolis, SC, Brazil, November 5-8, 2017.

correlation with the experimental data, giving similar stiffness. This good agreement of experimental data and finite element formulation is related to the geometric nonlinearity taken into account in the model, which is not taken into account in the theoretical model.

In the Fig. 8 and 9 the deformed configuration of beam (1 and 2 respectively) are presented (considering the load F = 9 kN). The Fig. 8 and 9 show the correct coupling between connectors displacements (particles) and composite timber-concrete displacements (matrix), which is the main feature of particulate FEM model.

3.3 Longitudinal Stress analysis

Figures 10 and 11 present the longitudinal stress diagram of beams 1 and 2, respectivelly. It should be noticed that for the theoretical model most of the concrete slab is under compression and there is a part of it in tension, while most of timber joist is under tension.

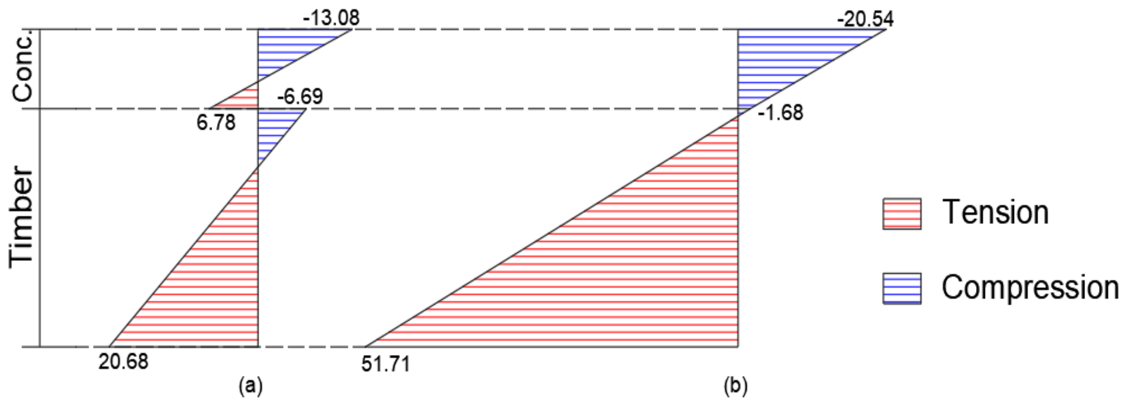

Figure 10. Longitudinal stress diagram of the beam 1 obtained by: a) theoretical model and b) finite element formulation (unit: 10^3 kN/m²)

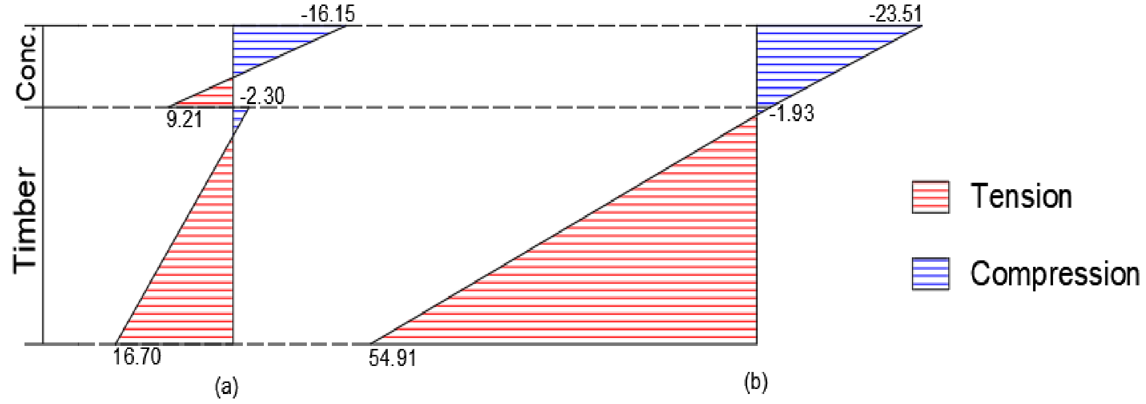

Figure 11. Longitudinal stress diagram of the beam 2 obtained by: a) theoretical model and b) finite element formulation (unit: 10^3 kN/m²)

By the longitudinal stress diagram obtained with the finite element formulation can be noticed that the entire concrete slab is in compression and almost all of the timber joist is in tension. This was expected, since the basic principle of working of the composite timber-concrete beams is that the concrete works essentially in compression and timber in tension, taking advantage of the main qualities of these materials in bending.

It also can be noticed by these figures the difference between the theoretical model and the finite element formulation. For the beam 1, the compression in the upper part of the concrete slab obtained by the finite element formulation is 57% greater than that obtained by the theoretical model, the tension in the bottom of the timber joist calculated by the finite element formulation is 150% greater than that obtained by the theoretical model. For the beam 2, the compression in the upper part of the concrete slab obtained by the finite element formulation is 45% greater, while the tension in the bottom of the timber is 228% greater. Since more rigid structures leads to lower stresses, and the results presented by the theoretical model are stiffer than the obtained by the finite element formulation, this was already expected.

Another difference in the results of the theoretical model and the finite element formulation is in the joint of the concrete slab and the timber joist. By results obtained with the finite element formulation, the upper part of the timber joist and the lower part of the concrete slab are submitted to the same stress. On the other side, the stresses in the upper part of the timber and the lower part of the concrete in the theoretical model are different, being the concrete in tension and the timber in compression. This behavior can be explained by the different approaches used by the methods: while the theoretical model allows the slip between the concrete and timber surfaces through of slip modulus, Eq. (30), while the finite element formulation considers the total interaction of the materials.

4 CONCLUSION

With the obtained results, we concluded that the use of FEM particulate model with the consideration of the geometric nonlinearity is a good approach to represent the behavior of timber-concrete composites beams. The evolution of the vertical displacement with the force is well represented by the formulation, leading to results close to experimental data. On the other hand, the theoretical model proposed to the European standardization, Eurocode 5 (2004), give more rigid results.

The stresses given by the theoretical model and the finite element formulation are quite different. The results obtained by the FEM particulate model are greater than the acquired by the theoretical model, due to greater stiffness of the theoretical model. In consequence of the greater stiffness and the lower stresses values, we can say that the model proposed by the European standardization may under evaluate imposed stresses in this condition.

It was observed that the formulation is not capable of represent the discontinuity in stresses in the surface of connection of the timber and concrete so far. So, for future works, it is proposed the consideration of the slip between the materials, thus being able to represent the discontinuity of the stresses in the region of interaction of the materials.

ACKNOWLEDGEMENTS

The authors thanks CNPq (Nacional Council for Scientific Research and Development) and CAPES (Coordination of Improvement of Higher Level Personnel) for the support given in this research.

REFERENCES

Dias, A.M.P.G., 2005. *Mechanical behaviour of timber-concrete joints.* PhD thesis, University of Coimbra.

Dias, A.M.P.G., Van de Kuilen, J.W., Lopes, S., & Cruz, H., 2007. A non-linear 3D FEM model to simulate timber-concrete joints. *Advances in Engineering Software*, vol. 38, pp. 522-530.

Dias, A.M.P.G., Cruz, H.M.P., Lopes, S.M.R., Van de Kuilen, J.W., 2010. Stiffness of dowel-type fasteners in timber-concrete joints. *Structures and Buildings*, vol. 163, pp. 257-266.

Dias, A.M.P.G., Jorge, L.F.C., 2011. The effect of ductile connectors on the behaviour of timber-concrete composite beams. *Engineering Structures*, vol. 33, pp. 3033-3042.

EUROPEAN COMMITTEE FOR STANDARDIZATION. EN-1995-1-1: Eurocode 5: Design of Timber Structures – Part 1-1: General – Common rules and rules for buildings, 2004.

Matthiesen, J.A., Alcântra Segundinho, P.G. de, Molima, J.C., & Carreira, M. R., 2010. Performance of metallic connectors in timber-concrete composite beams in the service limit state. *Minerva – Pesquisa e Tecnologia*, vol. 7, pp. 79-89. *(in Portuguese)*

Molina, J.C., 2008. *Analysis of the dynamic behavior of the connection formed by bonded steel bars for composite timber-concrete bridges.* PhD thesis, University of São Paulo. *(in Portuguese)*

Molina, J.C., & Calil Junior, C., 2009. Strategy for numeric modelling of composite systems considering different models of rupture for the materials. *Ingeniare – Revista chilena de ingeniería*, vol. 17, n. 2, pp. 256-266. *(in Portuguese)*

Paccola, R. R., & Coda, H. B., 2016. A direct FEM approach for particulate reinforced elastic solids. *Composite Structures*, vol. 45, pp. 235–251.

Sebastian, W., 2003. Ductility requeriments in connections of composite flexural structures. *International Journal of Mechanical Sciences*, vol. 38, pp. 522-530.

Yeoh, D., Fragiacomo, M., Franceschi, M., & Boon, K.H., 2011. State of the Art on Timber-Concrete Composite Structures: Literature Review. *Journal of Structural Engineering,* vol. 137, n. 10, pp. 1085-1095.